Formation of hexagonal and cubic ice during low-temperature growth

Konrad Thürmer[1] and Shu Nie

Sandia National Laboratories, Livermore, CA 94550

Edited by Andrew Hodgson, University of Liverpool, Liverpool, United Kingdom, and accepted by the Editorial Board May 28, 2013 (received for review February 15, 2013)

From our daily life we are familiar with hexagonal ice, but at very low temperature ice can exist in a different structure—that of cubic ice. Seeking to unravel the enigmatic relationship between these two low-pressure phases, we examined their formation on a Pt (111) substrate at low temperatures with scanning tunneling microscopy and atomic force microscopy. After completion of the one-molecule-thick wetting layer, 3D clusters of hexagonal ice grow via layer nucleation. The coalescence of these clusters creates a rich scenario of domain-boundary and screw-dislocation formation. We discovered that during subsequent growth, domain boundaries are replaced by growth spirals around screw dislocations, and that the nature of these spirals determines whether ice adopts the cubic or the hexagonal structure. Initially, most of these spirals are single, i.e., they host a screw dislocation with a Burgers vector connecting neighboring molecular planes, and produce cubic ice. Films thicker than ∼20 nm, however, are dominated by double spirals. Their abundance is surprising because they require a Burgers vector spanning two molecular-layer spacings, distorting the crystal lattice to a larger extent. We propose that these double spirals grow at the expense of the initially more common single spirals for an energetic reason: they produce hexagonal ice.

ice growth mechanisms | molecular surface steps | molecular-layer nucleation | scanning probe microscopy | spiral growth

Owing to its ubiquity in nature, ice and its structural properties have inspired widespread interest (1, 2). Not long after the introduction of X-ray diffraction in 1912, the structure of the most common modification of ice, hexagonal ice Ih, had already been investigated extensively (1–6). In 1942, König (7) discovered that at low temperatures water occasionally crystallizes into a different modification, cubic ice Ic. Subsequently, cubic ice has been produced in the laboratory, e.g., by condensing water vapor onto cooled substrates (7–11), by heating amorphous solid water (7–9), by supercooling liquid water droplets (12–14) or clusters (15), or by freezing high-pressure phases of ice and reheating them at atmospheric pressure (16–19). Cubic ice has been proposed to also occur naturally, e.g., in the earth's atmosphere (13, 20–24) and in comets (25, 26). However, even after thousands of articles dedicated to ice formation have appeared, important questions regarding fundamental growth mechanisms of ice remain. Some of these questions concerning the competition between the two low-pressure crystalline phases ice Ih and ice Ic are addressed in this paper.

Ice Ih and ice Ic have been observed to coexist at temperatures up to 240 K (10–12, 18, 27, 28). When ice Ic is heated above 170 K it transforms irreversibly into ice Ih. The release of a measurable amount of heat (on the order of 35 J/mol) (17–19) establishes hexagonal ice as the equilibrium structure above 170 K. Below 170 K no phase transformation has been observed, allowing for the possibility that at these low temperatures cubic ice is energetically preferred (1, 29). Johari (27) argues that contributions from grain-boundary, interphase, and strain energies suppress the formation of hexagonal ice in bulk cubic ice. More recently, he proposed (30) that a lower interfacial energy favors the cubic versus the hexagonal structure for water droplets with radii smaller than 15 nm and for films less than 10 nm thick.

Our work aims at elucidating the complex relationship between these two ice phases by providing real-space information at the molecular scale. In apparent contradiction with Johari's argument (30), our previous scanning tunneling microscopy (STM) study (31) on ice/Pt(111) suggests that films thinner than 3 nm are mostly ice Ih, whereas cubic ice is favored in thicker films. In this earlier work we proposed that growth via nucleation of molecular layers leads to ice Ih; we now describe a dedicated nucleation experiment that yields conclusive evidence for this mechanism. Furthermore, in our earlier experiments we expanded the reach of STM from the previous limit of 1-to-2-nm-thick ice films to thicknesses up to ∼10 nm. In this paper, by introducing qPlus-sensor atomic force microscopy (AFM) (32, 33) into ice research, we are able to explore uncharted territory: ice films of unlimited thickness can now be imaged with molecular-layer resolution. AFM on thicker-than-20-nm ice revealed an unanticipated mechanism: growth in these thicker ice films occurs mainly via double spirals that produce hexagonal ice. Thus, by combining STM and AFM experiments we now provide a more comprehensive account of the mechanisms leading to hexagonal or cubic ice.

Preparing and Imaging Ice Films

We prepared and analyzed the ice films in a UHV chamber with a base pressure of $<3 \times 10^{-11}$ mbar. The films were deposited at a rate of ∼1 Å/min by directing water vapor onto the platinum sample held at 140–145 K. For the nucleation experiments, the ice film was subsequently cooled; 2D islands were grown at 115 K and annealed at 125 K for 2 h. After each deposition a small non-evaporable-getter pump in line of sight to the sample surface was used to decrease the pressure near the sample. There are no indications that our measurements were affected by contaminants (see *SI Text*, section S1 for details).

Films up to 10 nm thick were imaged nondestructively (31, 34) with STM at $T < 120$ K, using a sample bias of ∼−6 V and a tunnel current of ∼0.4 pA. At larger thicknesses STM becomes destructive and we had to rely on AFM. Donev et al. (35), using beam-deflection AFM in a commercial setup similar to ours (Omicron variable-temperature scanning probe microscope, SPM), found that the contact mode modifies the ice films, whereas the noncontact mode leaves them intact. The resolution of the noncontact mode, however, was not sufficient to distinguish between cubic and hexagonal ice. To overcome these limitations we used qPlus-sensor AFM (32, 33) for imaging films thicker than 10 nm. The qPlus sensor was operated at a resonance frequency of 22.5 kHz with the feedback set at $\Delta f = -3$ Hz. Fig. 1 demonstrates that qPlus AFM can

Author contributions: K.T. designed research; S.N. codesigned nucleation experiments; K.T. and S.N. performed research; K.T. analyzed data; and K.T. wrote the paper.

The authors declare no conflict of interest.

This article is a PNAS Direct Submission. A.H. is a guest editor invited by the Editorial Board.

[1]To whom correspondence should be addressed. E-mail: kthurme@sandia.gov.

This article contains supporting information online at www.pnas.org/lookup/suppl/doi:10.1073/pnas.1303001110/-/DCSupplemental.

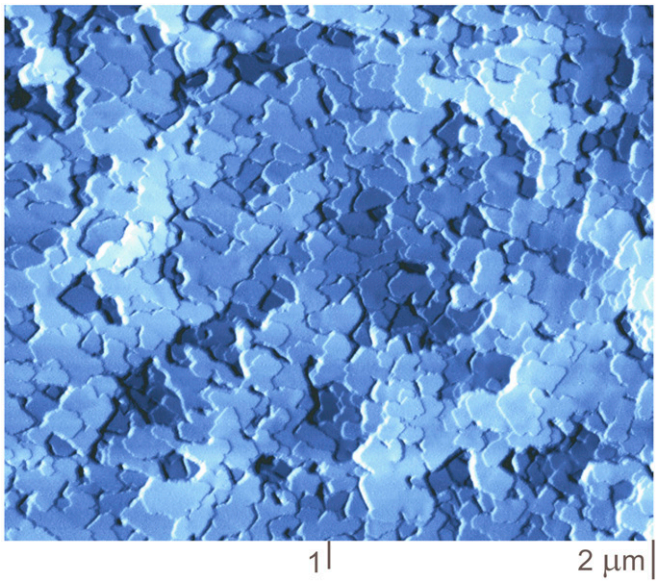

Fig. 1. AFM image showing the rich surface topography of a 20-nm-thick film of ice grown onto Pt(111) at 140 K. Molecular surface steps can be resolved nondestructively with AFM using the qPlus sensor technique.

nondestructively resolve molecular surface steps on thick ice films. This 2-μm-wide image of 20-nm-thick ice grown at 140 K illustrates the complexity of the film morphology. In the remainder of this paper it will become clear that the ability to resolve molecular surface steps is crucial to unravel this complexity and determine the mechanisms leading to hexagonal or cubic ice.

Results and Discussion

As reported by Kimmel et al. (36) and confirmed by our previous STM work (31), water deposited at 135–150 K onto Pt(111) first forms a one-molecule-thin wetting layer (37–40). Then, isolated 3D ice crystallites emerge and eventually, at thicknesses of ~3–10 nm, coalesce into a continuous multilayer film. (Three-dimensional crystallites embedded in a 2D wetting layer are also found when amorphous ice is heated to 150 K, as reported in Waluyo et al. in ref. 41.) In the following we discuss the growth mechanisms associated with the different thickness regimes, and relate them to the formation of either cubic or hexagonal ice.

Cubic and Hexagonal Ice Structure. To interpret the surface morphology we first recall the molecular structure (1, 2) of the two ice phases Ih and Ic shown schematically in Fig. 2. Both structures have in common that the oxygen atoms are arranged in corrugated honeycomb layers (bilayers) held together by hydrogen bonds. Neighboring bilayers connect via H bonds between the lower O atoms of the higher layer and the higher O atoms of the lower layer (Fig. 2 *A* and *B*). Within these bilayers, each higher-lying oxygen atom binds to three neighboring lower-lying oxygen atoms, forming a triangle (Fig. 2*C*), which we call "stacking triangle." In the cubic-ice lattice, where the oxygen atoms are arranged in the diamond structure, all bilayers are identical and their stacking triangles point in the same direction. The hexagonal-ice lattice can be obtained from the cubic-ice lattice by azimuthally rotating every other bilayer by 180°. Hence, in hexagonal ice the orientation of the stacking triangles alternates from layer to layer. Throughout the paper we use a color coding (green and blue) to distinguish the two types of intrabilayer stacking corresponding to the two stacking-triangle orientations.

Growth via Nucleation. At the early stage of multilayer growth the ice films comprise isolated 3D crystallites embedded in a 2D wetting layer (34, 36). Because their flat top facets lack step-producing defects where the deposited water could readily attach, the crystals can only increase their height by nucleating new molecular layers (Fig. 3*A*). We had previously proposed (31) that such nucleation produces hexagonal ice, although our experimental evidence based on as-grown films was indirect. Here, we report an experiment dedicated to determine the type of ice produced via nucleation. Our approach exploits the fact that 2D islands grown on ice films thinner than ~5 nm exhibit pronounced triangular shapes (42) reflecting their intrabilayer stacking. First, large triangular 2D structures are grown that serve as templates with known intrabilayer stacking. Such triangular templates can be found on as-grown continuous 3-nm-thick films deposited at 145 K. Then, small triangular islands, nucleated on top of these templates, reveal via their orientation whether or not the intralayer stacking alternates from layer to layer. The schematic in Fig. 3*B* illustrates both cases: island 1 represents alternating stacking as in hexagonal ice, and island 2 corresponds to uniform stacking as in cubic ice. To create suitable arrays (43) of small triangular islands we deposit a fraction of a monolayer of water at 115 K and anneal the sample at 125 K for 2 h. The STM image of Fig. 3*C* reveals the unambiguous result: All 8 triangular islands grown on the downward-pointing triangular template (green) are pointing upward,

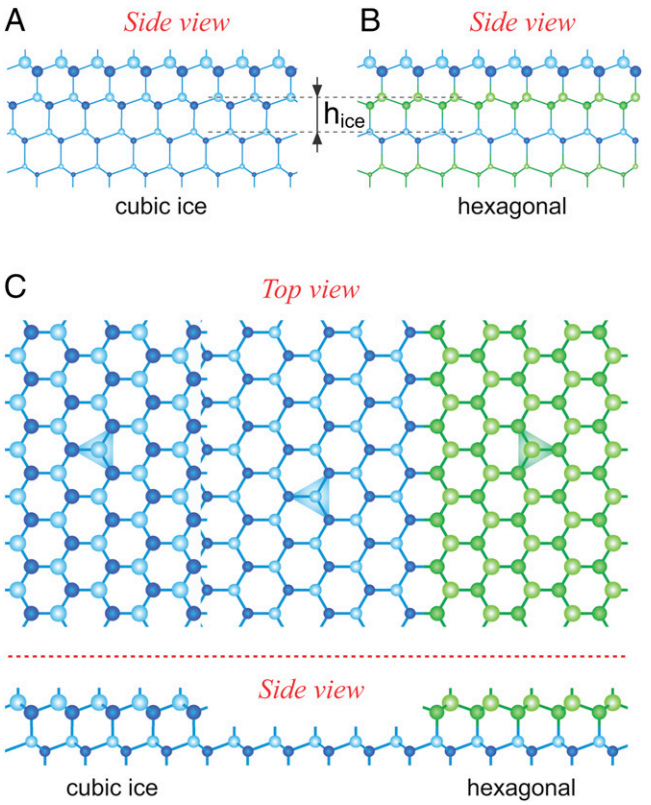

Fig. 2. Schematic comparison of the lattices of the two crystalline low-pressure ice structures, cubic and hexagonal ice. The oxygen atoms (circles) are connected via H bonds (lines). Higher-lying atoms are represented by larger circles. (*A* and *B*) Side views of four bilayers of cubic and hexagonal ice. (*C*) (*Upper*) Top view of an ice bilayer (*Middle*, blue, small circles) that is covered by a partial bilayer according to the stacking in cubic ice (*Left*, blue, large circles) and by a partial bilayer according to hexagonal-ice stacking (*Right*, green, large circles). (*Lower*) Side view of this arrangement. Within each bilayer the higher oxygen atoms are surrounded by three lower-lying oxygen atoms forming triangles (green or blue) representing the intrabilayer stacking. The orientation of these stacking triangles alternates from layer to layer in hexagonal ice but not in cubic ice.

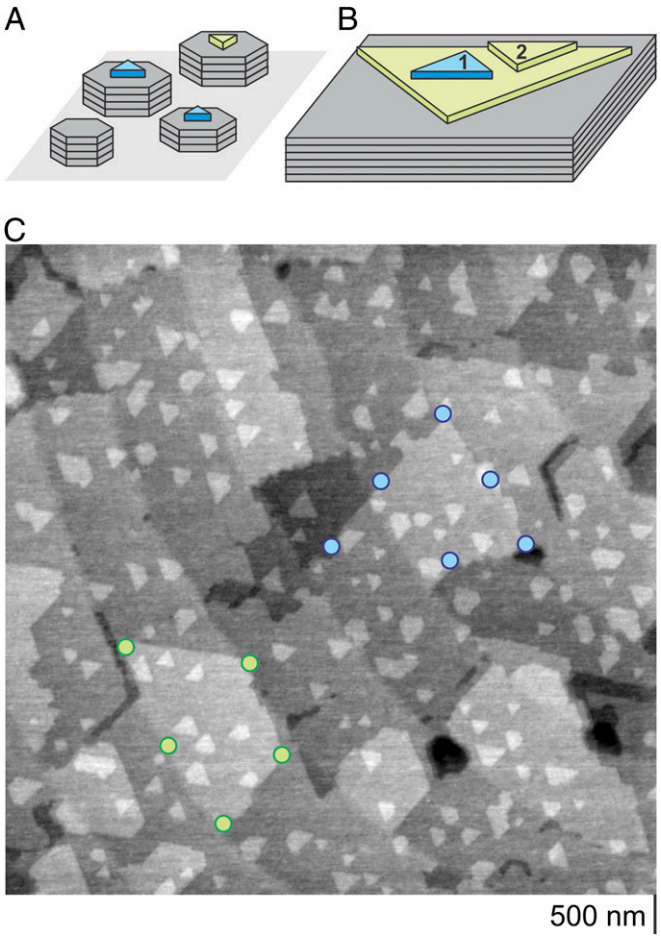

Fig. 3. Ice growth via nucleation. (*A*) Schematic of isolated crystals that can only increase their height by nucleating new molecular layers on their top facets. (*B*) Schematic of the experiment to test whether growth via nucleation leads to cubic or hexagonal ice. The two orientations of the triangular 2D islands reflect the two possible ways of intralayer stacking (blue or green). Alternating island orientation (case 1) corresponds to alternating intralayer stacking as in hexagonal ice. Uniformly oriented triangles (case 2) are expected for cubic ice. (*C*) STM image of a 3-nm-thick ice film grown at 145 K, decorated by an array of small 2D islands nucleated at 115 K and annealed at 125 K. Upward-pointing triangles nucleate on downward-pointing features (green) and vice versa (blue), providing evidence that growth via nucleation leads to hexagonal ice.

and all 10 islands on the upward-pointing template (blue) point downward, i.e., all nucleated islands are rotated with respect to their templates. Relating the alternating island orientations to alternating intrabilayer stacking, we can thus conclude that growth via nucleation leads to hexagonal ice. This conclusion is consistent with the observation that isolated 3D crystallites, which had to grow via nucleation, tend to be more hexagonally shaped (34) than 2D islands grown on films of comparable thickness (42).

Spiral Growth. We now discuss the growth situation that arises after the 3D crystallites have coalesced into a continuous film. Previously we had shown that the coalescence of these crystallites across substrate steps generates screw dislocations, which produce surface steps that allow spiral growth without nucleation (31). At film thicknesses accessible with STM, i.e., <10 nm, these spirals mostly lead to cubic ice. Our current study, which includes AFM measurements at larger thicknesses, reveals a richer behavior: at thicknesses ~10–20 nm, a different type of growth spiral emerges and becomes dominant, causing the growth to revert from cubic to hexagonal ice formation.

Let us first summarize the processes leading to the formation of cubic ice at thicknesses between ~4 and ~15 nm (for more details see ref. 31). In Fig. 4 *A–D*, depicting a typical scenario, the molecular layers are color-coded according to their intralayer stacking. The layers in Fig. 4*A* alternate between "green" and "blue," consistent with the hexagonal structure of isolated crystallites. Crystallites with different stacking sequences (crystals 1 and 2 in Fig. 4*A*) do not readily merge but form domain boundaries (marked "db") instead. Individual crystallites (crystal 3) do not typically overgrow substrate steps, rendering this a likely location where coalescence occurs. The molecular layers of crystallites facing each other across a substrate step are vertically offset from each other by the height of the substrate step, which is, for Pt(111) and many other materials, roughly half the spacing h_{ice} between the molecular ice layers. Crystallites merging across a substrate step bend to join layers with equal intralayer stacking, i.e., crystal 1 bends downward and crystal 2 bends upward to connect to crystal 3, resulting in a screw dislocation that produces a surface step (Fig. 4*B*). Evidently, deposited water can attach to this step and bury the domain boundary (Fig. 4*C*). The top layer can now readily advance and create a growth spiral (Fig. 4*D*). The subsequent growth proceeds by expanding this green top layer, thereby producing ice of uniform intralayer stacking, i.e., cubic ice. Our previous STM experiments (31) examining films grown at 135–150 K support this scenario. Configurations equivalent to Fig. 4*B* are ubiquitous in films shortly after coalescence; for

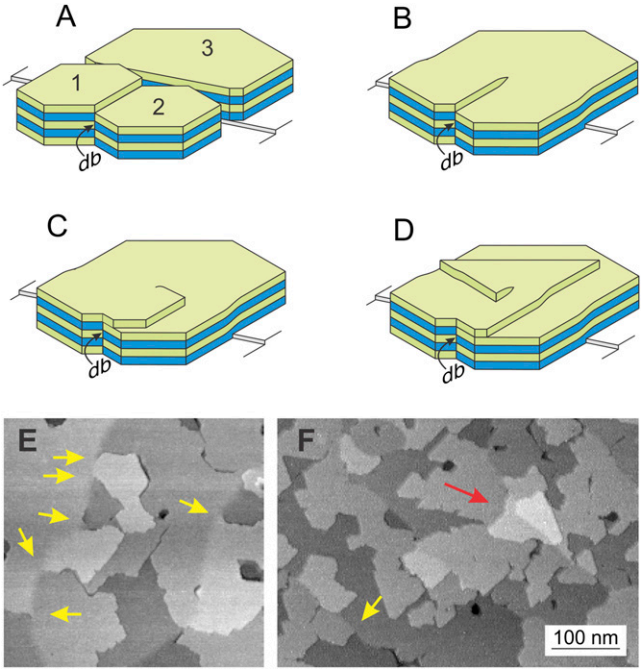

Fig. 4. Spiral growth of cubic ice. (*A–D*) Scenario of how the coalescence of three crystallites across a substrate step can form a growth spiral producing cubic ice. (*A*) Individual crystallites expand until encountering a substrate step (crystal 3) or a neighboring crystal (crystals 1 and 2). These crystals can merge if their intralayer stacking matches or, as in the case of crystals 1 and 2, form a domain boundary (labeled db). (*B*) The substrate step height is roughly one-half the ice-bilayer spacing ($h_{Pt} = 0.62\ h_{ice}$). According to their stacking the ice crystals bend upward (crystal 2) or downward (crystal 1) to connect matching layers across a substrate step, creating a screw dislocation. Material can attach to the resulting surface step, thus overgrowing the domain boundary and expanding the top layer (*C*). The resulting growth spiral (*D*) generates ice of uniform intralayer stacking (green in this example), i.e., cubic ice. (*E* and *F*) STM images of a 9-nm-thick (*E*) and a 4-nm-thick (*F*) ice film grown at 140 K, showing configurations matching that of *B* marked by yellow arrows, and that of *D* marked by a red arrow.

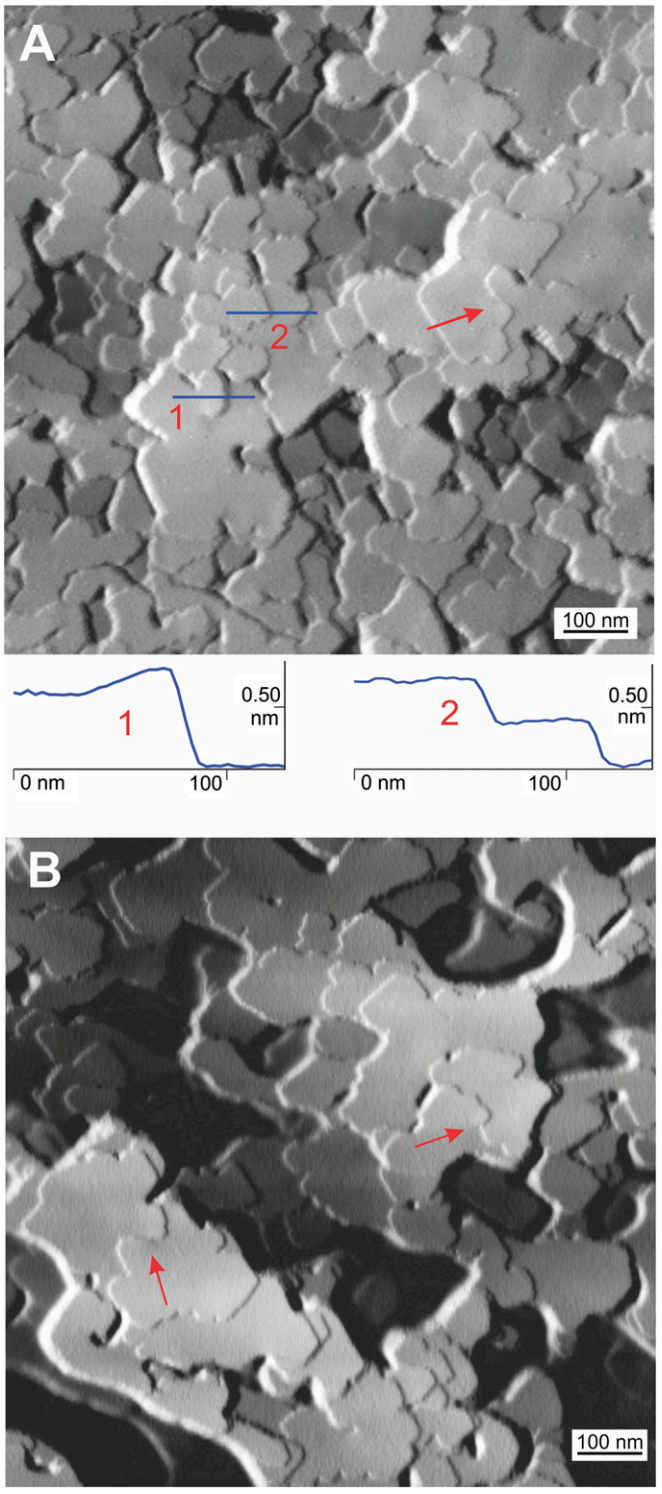

Fig. 5. AFM images of double spirals in thicker ice films. (*A*) Enlarged 1-μm^2 region of the 20-nm-thick film shown in Fig. 1. The arrow marks an S-shaped double spiral. Below are height profiles cutting through a step loop of double height (marked 1) and, for comparison, through two regular steps of single height (marked 2). (*B*) A 1-μm^2 image of a 40-nm (~100 bilayers)-thick film. Two double spirals (red arrows) are the most prominent features.

some examples follow the yellow arrows in Fig. 4*E*. Some of these configurations develop into spirals equivalent to Fig. 4*D*; an example is shown in Fig. 4*F* marked by a red arrow (for more STM data see ref. 31).

Does cubic-ice formation via growth spirals extend to films thicker than STM's reach? And, is hexagonal ice created only during the initial stage, where growth proceeds via layer nucleation? AFM, capable of imaging molecular surface steps of ice non-destructively, is well suited to address these questions. Examining films up to ~100 molecular layers thick, we found that their surface morphology differs markedly from those of the thinner films studied previously with STM. Fig. 5*A* displays a representative 1-μm^2 region of a 20-nm-thick ice film grown at 140 K. (This image is a zoom into the lower-right portion of Fig. 1.) The morphology is clearly not dominated by the simple, often triangular-shaped spirals found in films thinner than 10 nm. Instead, especially in the highest surface areas, we find features that were not present in thinner films. One, marked by an arrow, is an S-shaped step at the center of a double spiral. Another feature, labeled "1," has, at first sight, the appearance of a simple growth spiral. However, comparing its profile with those of single molecular surface steps (labeled "2") reveals that its step has twice their height. Thus, it too is at the center of a double spiral, although here the two steps are very close together. Overall, the morphology is very complex, rendering it difficult to estimate the fraction of growth that proceeds via double spirals. The situation simplifies somewhat with increasing film thickness: Images of 40-nm-thick ice (Fig. 5*B*) reveal a morphology dominated by double spirals, which have now risen several nanometers above their surroundings. We conclude that a substantial portion of growth occurs via double spirals in these thicker ice films.

What effect do these double spirals have on the crystal structure? Fig. 6 *A*–*C* illustrates graphically that a double spiral is associated with a screw dislocation with a double Burgers vector, i.e., the length of the Burgers vector's normal component is twice the spacing h_{ice} between molecular layers. In contrast with a single

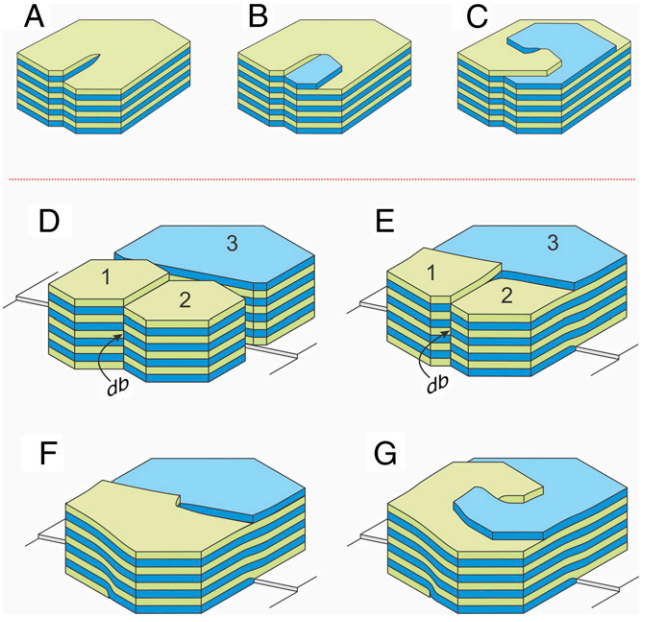

Fig. 6. Schematics of double spirals that produce hexagonal ice. (*A*–*C*) Double spirals are created by screw dislocations with a double Burgers vector, i.e., a vector twice as long as the interlayer spacing. (*D*–*G*) Possible scenario leading to a double spiral, in which crystallites 1, 2, and 3 coalesce across a substrate step. Connecting the layers of crystals 1 and 2 to matching layers of crystal 3 creates two surface steps above the buried substrate step (*E*). The domain boundary (db) between crystals 1 and 2 can be eliminated by bending the crystals so that matching layers join *F*. The green and the blue top layer can now freely expand and twist around each other to form a double spiral that generates ice with alternating intralayer stacking, i.e., hexagonal ice.

spiral, which always generates ice of uniform intralayer stacking (Fig. 4 *B–D*), a double spiral propagates the intralayer stacking of two molecular layers. If those differ, i.e., one is blue and the other green, the film grows with alternating intralayer stacking, resulting in hexagonal ice. Thus, double spirals provide a kinetic route of growing hexagonal ice without nucleating new layers.

Envisioning an atomistic scenario leading to the configuration of Fig. 6 *A–C* via growth from water vapor is difficult. However, as in the single-spiral case of Fig. 4 *A–D*, coalescence of crystallites across substrate steps could be the key to the creation of double spirals as well. Fig. 6 *D–G* illustrates one of the various possible scenarios. To connect to matching layers of crystal 3, crystal 1 has to bend upward by $h_{Pt} \sim 2.26$ Å and crystal 2 downward by $h_{ice} - h_{Pt} \sim 1.4$ Å (Fig. 6*E*). The fate of this configuration will be decided at the domain boundary (labeled db). If the blue top layer of crystal 3 advances over crystal 2 and then stops at the domain boundary, the green top layer of crystal 1 will be the only remaining layer with a surface step and thus able to expand, resulting in a single spiral that produces cubic ice. (This scenario is shown in fig. 9 in ref. 31.) If, however, the layers (or at least the top layers) of crystal 2 bend upward by h_{ice} to connect to the matching layers of crystal 1 (Fig. 6*F*), the domain boundary is eliminated and both top layers (green and blue) can expand and wind around each other (Fig. 6*G*), forming a double spiral that produces hexagonal ice. The fact that domain boundaries vanish as films grow thicker is plausible because, whereas the elastic-energy cost due to bending the layers increases only logarithmically with film thickness, the energy gain of eliminating a vertical domain boundary increases linearly (see *SI Text*, section S2 for details). Each turn, a molecular layer rises by 1 molecular-layer spacing h_{ice} as it crosses the healed domain boundary and by another spacing h_{ice} $(= h_{Pt} + (h_{ice} - h_{Pt}))$ as it crosses the buried substrate step twice, hence the double Burgers vector. The relatively simple scenario of Fig. 6 *D–G* should be viewed as a prototype of other processes leading to double spirals.*

Although a few single spirals, obscured by rich morphology, might still exist in lower surface regions of Figs. 1 and 5, the dominance of hexagonal-ice-producing double spirals in thicker films is unmistakable. This observation is consistent with Glebov et al.'s (44) claim that their He atom scattering signal on 100-nm-thick ice/Pt(111) originates from hexagonal ice. The prevalence of double spirals at larger film thicknesses is surprising because they are difficult to form: due to their double Burgers vector, double spirals have a roughly 4 times larger elastic-energy cost (45) than single spirals. An additional obstacle in creating a double spiral is that matching layers must fuse "correctly" across a domain boundary despite the large height offset h_{ice} (Fig. 6*E*). Overcoming this large height offset requires the ice layers to bend considerably, which is energetically favorable only above a certain threshold film thickness (*SI Text*, section S2). Also, crystal 2 could connect with equal probability to matching layers of crystal 1 by bending downward by h_{ice}, instead of bending upward. This "incorrect" layer fusion would eliminate the domain boundary without creating any growth spiral. The fact that single spirals are easier to form than double spirals suggests the following scenario: At intermediate film thicknesses shortly after coalescence, most spirals are single, consistent with STM observations. (More precisely, we never observed double spirals at film thicknesses below 15 nm. The ability of SPM, however, to survey large surface areas is limited.)

At larger film thicknesses, a small number of double spirals will form to eliminate domain boundaries. Because there is substantial mass transport via surface diffusion at these growth temperatures (43), water molecules can detach from one spiral and attach to another. Hence, at a growth stage where single and double spirals are present, there will be a significant material exchange between both types of spirals. The net flux in this ripening process will be from spirals associated with the less stable ice toward spirals that produce equilibrium ice. The fact that the initial dominance of single spirals is followed by a dominance of double spirals in thicker films suggests that hexagonal-ice-producing double spirals grow at the expense of cubic-ice-producing single spirals. This adds experimental support to the idea that the hexagonal structure is more stable than the cubic structure also at these low temperatures.

The scenario presented above is meant to describe the essence of overall film evolution. As the AFM images of Figs. 1 and 5 illustrate, the morphology of real films is exceedingly complex, presumably due to intricate interactions of domain boundaries, substrate steps, dislocations, and stacking faults. For example, more complex stacking sequences equivalent to mixtures (11 ,14, 46) of hexagonal and cubic ice are expected to appear in film regions that are swept by surface steps originating in different growth spirals. On rough substrates ice can grow with even more degrees of freedom. Given this complexity, many questions concerning the transition between cubic and hexagonal ice have yet to be explored. In this endeavor, the ability to track large sample regions with good time resolution will be crucial, either by increasing AFM's scan speed without modifying the delicate ice, or by using inherently fast techniques.

Recently, optical microscopy succeeded in visualizing molecular steps on the basal plane of ice at ambient conditions (47, 48). Some of the imaged steps were attributed to growth spirals emerging from screw dislocations located at grain boundaries. Although the data did not resolve the nature of the spiral cores, we expect these spirals to be double because single spirals would lead to cubic ice, which should not occur at $T > 240$ K.

Conclusions

The ability to resolve molecular surface steps on ice films of any thickness proved an invaluable asset in identifying thickness-dependent growth mechanisms. STM and AFM images reveal that the crystal structure of ice, deposited at low temperatures (~140 K) onto Pt(111), switches twice as films grow thicker. Isolated 3D clusters, which can only grow via layer nucleation, consist of hexagonal ice. Following coalescence, cubic ice is produced in growth spirals created by screw dislocations above substrate steps. Eventually, at thicknesses of ~20 nm, a different type of growth spiral, generated by dislocations with a double Burgers vector, becomes dominant, causing the preferential formation of hexagonal ice. We expect this behavior to be widespread because many materials can play the specific role of the substrate in the described mechanisms, i.e., to facilitate spiral formation by providing surface steps of a height different from the spacing h_{ice} between molecular ice layers. The fact that film growth reverts from cubic to hexagonal ice despite the larger lattice distortion associated with double spirals argues for ice Ih being the equilibrium structure also at temperatures below 170 K, where cubic ice has not been observed to transform into hexagonal ice.

*In the example configuration of Fig. 6 all precoalescence crystallites consist of hexagonal ice. Similar scenarios can be constructed with some or all of the precoalescence crystallites having the cubic structure. In this case, crystallites of both types of intralayer stacking have to be involved. Grain boundaries between those nonmatching crystallites will remain and have to be overgrown by the expanding top layers. Also, a configuration equivalent to that of Fig. 6 *D–G* could be obtained by placing crystals 1 and 2 and the domain boundaries on the upper and crystal 3 on the lower terrace.

ACKNOWLEDGMENTS. We thank Norman C. Bartelt for insightful discussions. This research was supported by the Office of Basic Energy Sciences, Division of Materials Sciences, US Department of Energy (DOE) under Contract DEAC04-94AL85000; and by the Laboratory Directed Research and Development Program at Sandia National Laboratories, a multiprogram laboratory managed and operated by Sandia Corporation, a wholly owned subsidiary of Lockheed Martin Corporation, for the US DOE's National Nuclear Security Administration under Contract DE-AC04-94AL85000.

1. Hobbs PV (1974) *Ice Physics* (Clarendon, Oxford).
2. Petrenko VF, Whitworth RW (1999) *Physics of Ice* (Oxford Univ Press, Oxford).
3. Rinne F (1917) Das Kristallsystem und das Achsenverhaltnis des Eises [The crystal system and the axial ratio of ice]. *Ber Verh Sachs Acad Wiss, Math- Phys* 69:57–62.
4. Bragg WH (1922) The crystal structure of ice. *Proc Phys Soc London* 34:0098–0103.
5. Bernal JD, Fowler RH (1933) A theory of water and ionic solution, with particular reference to hydrogen and hydroxyl ions. *J Chem Phys* 1(8):515–548.
6. Pauling L (1935) The structure and entropy of ice and of other crystals with some randomness of atomic arrangement. *J Am Chem Soc* 57(12):2680–2684.
7. König H (1944) A cubic modification of ice. *Z Kristallogr* 105(4):279–286.
8. Honjo G, Kitamura N, Shimaoka K, Mihama K (1956) Low temperature specimen method for electron diffraction and electron microscopy. *J Phys Soc Jpn* 11(5):527–536.
9. Blackman M, Lisgarten ND (1957) The cubic and other structural forms of ice at low temperature and pressure. *Proc R Soc London* A239(1216):93–107.
10. Shallcross FV, Carpenter GB (1957) X-ray diffraction study of the cubic phase of ice. *J Chem Phys* 26(4):782–784.
11. Kuhs WF, Sippel C, Falenty A, Hansen TC (2012) Extent and relevance of stacking disorder in "ice I(c)". *Proc Natl Acad Sci USA* 109(52):21259–21264.
12. Mayer E, Hallbrucker A (1987) Cubic ice from liquid water. *Nature* 325(6105):601–602.
13. Murray BJ, Knopf DA, Bertram AK (2005) The formation of cubic ice under conditions relevant to Earth's atmosphere. *Nature* 434(7030):202–205.
14. Malkin TL, Murray BJ, Brukhno AV, Anwar J, Salzmann CG (2012) Structure of ice crystallized from supercooled water. *Proc Natl Acad Sci USA* 109(4):1041–1045.
15. Huang JF, Bartell LS (1995) Kinetics of homogeneous nucleation in the freezing of large water clusters. *J Phys Chem* 99(12):3924–3931.
16. Bertie JE, Whalley E, Calvert LD (1963) Transformations of ice II, ice III, and ice V at atmospheric pressure. *J Chem Phys* 38(4):840–846.
17. McMillan JA, Los SC (1965) Vitreous ice - irreversible transformations during warm-up. *Nature* 206(4986):806–807.
18. Yamamuro O, Oguni M, Matsuo T, Suga H (1987) Heat-capacity and glass-transition of pure and doped cubic ices. *J Phys Chem Solids* 48(10):935–942.
19. Handa YP, Klug DD, Whalley E (1988) Energies of the phases of ice at low-temperature and pressure relative to ice Ih. *Can J Chem* 66(4):919–924.
20. Kobayashi T, Furukawa Y, Takahashi T, Uyeda H (1976) Cubic structure models at junctions in polycrystalline snow crystals. *J Cryst Growth* 35(3):262–268.
21. Whalley E (1981) Scheiners Halo - Evidence for ice Ic in the atmosphere. *Science* 211(4480):389–390.
22. Whalley E (1983) Cubic ice in nature. *J Phys Chem* 87(21):4174–4179.
23. Riikonen M, et al. (2000) Halo observations provide evidence of airborne cubic ice in the Earth's atmosphere. *Appl Opt* 39(33):6080–6085.
24. Murphy DM (2003) Dehydration in cold clouds is enhanced by a transition from cubic to hexagonal ice. *Geophys Res Lett* 30(23):2230.
25. Prialnik D, Bar-Nun A (1992) Crystallization of amorphous ice as the cause of comet P/Halley's outburst at 14 AU. *Astron Astrophys* 258(2):L9–L12.
26. Gronkowski P (2007) The search for a cometary outbursts mechanism: A comparison of various theories. *Astron Nachr* 328(2):126–136.
27. Johari GP (1998) On the coexistence of cubic and hexagonal ice between 160 and 240 K. *Philos Mag B-Phys Condens Matter Stat Mech Electron Opt Magn Prop* 78(4):375–383.
28. Hansen TC, Koza MM, Lindner P, Kuhs WF (2008) Formation and annealing of cubic ice: II. Kinetic study. *J Phys Condens Matter* 20(28):285105.
29. Ghormley JA (1968) Enthalpy changes and heat-capacity changes in transformations from high-surface-area amorphous ice to stable hexagonal ice. *J Chem Phys* 48(1):503–508.
30. Johari GP (2005) Water's size-dependent freezing to cubic ice. *J Chem Phys* 122(19):194504.
31. Thürmer K, Bartelt NC (2008) Growth of multilayer ice films and the formation of cubic ice imaged with STM. *Phys Rev B* 77(19):195425.
32. Giessibl FJ (2005) AFM's path to atomic resolution. *Mater Today* 8(5):32–41.
33. Giessibl FJ, Quate CF (2006) Exploring the nanoworld with atomic force microscopy. *Phys Today* 59(12):44–50.
34. Thürmer K, Bartelt NC (2008) Nucleation-limited dewetting of ice films on Pt(111). *Phys Rev Lett* 100(18):186101.
35. Donev JMK, Yu Q, Long BR, Bollinger RK, Fain SC, Jr. (2005) Noncontact atomic force microscopy studies of ultrathin films of amorphous solid water deposited on Au(111). *J Chem Phys* 123(4):044706.
36. Kimmel GA, Petrik NG, Dohnálek Z, Kay BD (2007) Crystalline ice growth on Pt(111) and Pd(111): Nonwetting growth on a hydrophobic water monolayer. *J Chem Phys* 126(11):114702.
37. Glebov A, Graham AP, Menzel A, Toennies JP (1997) Orientational ordering of two-dimensional ice on Pt(111). *J Chem Phys* 106(22):9382–9385.
38. Harnett J, Haq S, Hodgson A (2003) Electron induced restructuring of crystalline ice adsorbed on Pt(111). *Surf Sci* 528(1–3):15–19.
39. Nie S, Feibelman PJ, Bartelt NC, Thürmer K (2010) Pentagons and heptagons in the first water layer on Pt(111). *Phys Rev Lett* 105(2):026102.
40. Standop S, Redinger A, Morgenstern M, Michely T, Busse C (2010) Molecular structure of the H_2O wetting layer on Pt(111). *Phys Rev B* 82(16):161412.
41. Waluyo I, et al. (2008) Spectroscopic evidence for the formation of 3-D crystallites during isothermal heating of amorphous ice on Pt(111). *Surf Sci* 602(11):2004–2008.
42. Nie S, Bartelt NC, Thürmer K (2011) Evolution of proton order during ice-film growth: An analysis of island shapes. *Phys Rev B* 84(3):035420.
43. Nie S, Bartelt NC, Thürmer K (2009) Observation of surface self-diffusion on ice. *Phys Rev Lett* 102(13):136101.
44. Glebov A, Graham AP, Menzel A, Toennies JP, Senet P (2000) A helium atom scattering study of the structure and phonon dynamics of the ice surface. *J Chem Phys* 112(24):11011–11022.
45. Hirth JP, Lothe J (1992) *Theory of Dislocations* (Krieger, Malabar, FL).
46. Hansen TC, Koza MM, Kuhs WF (2008) Formation and annealing of cubic ice: I. Modelling of stacking faults. *J Phys Condens Matter* 20(28):285104.
47. Sazaki G, Zepeda S, Nakatsubo S, Yokoyama E, Furukawa Y (2010) Elementary steps at the surface of ice crystals visualized by advanced optical microscopy. *Proc Natl Acad Sci USA* 107(46):19702–19707.
48. Sazaki G, Asakawa H, Nagashima K, Nakatsubo S, Furukawa Y (2013) How do quasi-liquid layers emerge from ice crystal surfaces? *Cryst Growth Des* 13(4):1761–1766.

Supporting Information

Thürmer and Nie 10.1073/pnas.1303001110

SI Text

S1. Is the Growth of These Ice Films Affected by Contaminants from the Residual Gas? Deposition times of up to 7 h could, in principle, cause an accumulation of contaminants from the residual gas even at a background pressure in the low 10^{-11}-mbar range (1). However, the main constituents of the residual gas in our UHV system, H_2, CO, and CO_2, are known to desorb from ice well below our growth temperature (2–4). Also, the cold environment near the sample reduces the local pressure significantly below the main chamber pressure. The fact that ice growth under these conditions is not affected by contamination is evidenced by scanning tunneling microscopy (STM) measurements: Over the course of 38 h no change in the rate of surface diffusion could be detected (5), and after keeping the sample for several days in the STM stage, surface images show no hint of contamination.

S2. Comparing the Energy Cost of Bending Ice Layers with the Energy Gain of Eliminating a Domain Boundary. The energy cost of bending the ice layers upward by h_{ice} can be estimated by the strain field in the upper half space of a hypothetical step dislocation (6) with a Burger's vector $b = 2\,h_{ice} = 7.33$ Å. The elastic energy u_{bent} per length of a bent ice-film section (= length of the eliminated domain boundary) is thus half the energy of this step dislocation (7) $u_{bent} \sim u_{disl}/2 \sim \mu b^2/(8\pi(2 - E/2\mu)) \times \ln(4R/b)$, with the shear modulus μ, elasticity modulus E, and the outer radius R of the considered distortion field. Approximating the radius of the distorted region by the film thickness d and using the known values (8) for $\mu(T = 140\ \text{K}) = 4.1$ GPa and $E(T = 140\ \text{K}) = 10.8$ GPa yields $u_{bent} \sim 1.28 \times 10^{-10}\ \text{N} \times \ln(4d/b) = 0.079\ \text{eV/Å} \times \ln(2d/h_{ice})$.

For the scenario described in the main text to occur, the energy cost of bending ice layers has to be surpassed by the energy gained upon eliminating a domain boundary. The exact structure and energy of these domain boundaries created in the random process of coalescence is not known and is expected to vary somewhat. For a rough estimate we consider a domain boundary along the prism face of hexagonal ice Ih and assume its energy to be smaller but on the order of the total energy of the broken bonds of a bulk-truncated crystal. Accordingly, given that the energy per hydrogen bond is ∼0.3 eV (9), we use 0.1 eV per broken H bond for our estimate. With the intralayer separation between the broken bond of 4.5 Å, the energy per length of the domain boundary becomes $u_{db} \sim 0.1\ \text{eV}/4.5\ \text{Å} \times d/h_{ice} = 0.0222\ \text{eV/Å} \times d/h_{ice}$.

The thickness where u_{bent} equals u_{db} marks the threshold above which it becomes favorable to bend the ice layers and eliminate the domain boundary. $u_{bent} = u_{db}$ (i.e., $0.079\ \text{eV/Å} \times \ln(2d/h_{ice}) = 0.0222\ \text{eV/Å} \times d/h_{ice}$) occurs at $d_{thres} \sim 11 h_{ice} \sim 4$ nm. Given the used simplifying assumptions, this value of 4 nm only represents the order of magnitude of the threshold thickness. The actual threshold is probably slightly higher, around 15 nm, above which double spirals start to form. Using 38.3 meV per broken bond in the estimate of the domain-boundary energy, which is as reasonable as the initially assumed 100 meV, yields $d_{thres} = 15$ nm.

1. Kalff M, Comsa G, Michely T (1998) How sensitive is epitaxial growth to adsorbates? *Phys Rev Lett* 81(6):1255.
2. Amiaud L, et al. (2006) Interaction of D-2 with H2O amorphous ice studied by temperature-programed desorption experiments. *J Chem Phys (USA)* 124(9):094702.
3. Allouche A, Verlaque P, Pourcin J (1998) CO adsorption isotherms on ice by Fourier transform infrared spectroscopy and new insights of the ice surface from quantum ab initio investigations. *J Phys Chem B* 102(1):89–98.
4. Kim YK, Park SC, Kim JH, Lee CW, Kang H (2008) Interaction of carbon dioxide and hydroxide ion at the surface of ice films. *J Phys Chem C* 112(46):18104–18109.
5. Nie S, Bartelt NC, Thürmer K (2009) Observation of surface self-diffusion on ice. *Phys Rev Lett* 102(13):136101.
6. Thürmer K, Williams ED, Reutt-Robey JE (2003) Dewetting dynamics of ultrathin silver films on Si(111). *Phys Rev B* 68(15):155423.
7. Hirth JP, Lothe J (1992) *Theory of Dislocations* (Krieger, Malabar, FL).
8. Gammon PH, Klefte H, Clouter MJ (1983) Elastic-constants of ice samples by Brillouin spectroscopy. *J Phys Chem* 87(21):4025–4029.
9. Petrenko VF, Whitworth RW (1999) *Physics of Ice* (Oxford Univ Press, Oxford).